 doi:10.20944/preprints202208.0490.v1

Article

Inference of Pulmonary Arterial Pressure using Non-invasive Measurements and Scientific Machine Learning Techniques

Ryno Laubscher [1,] *, Johan van der Merwe[1], Philip Herbst [2] and Jacques Liebenberg [2]

[1] Department of Mechanical and Mechatronic Engineering; Stellenbosch University; South-Africa
[2] Division of Cardiology; Faculty of Medicine and Health Sciences; Stellenbosch University; South-Africa
* Correspondence: rlaubscher@sun.ac.za

Abstract: Reliable quantification of pulmonary arterial pressure is essential in the diagnostic and prognostic assessment of a range of cardiovascular pathologies including rheumatic heart disease, yet an accurate and routinely available method for its quantification remains elusive. This work proposes an approach to infer pulmonary arterial pressure based on scientific machine learning techniques and non-invasive, clinically available measurements. A 0-D multicompartment model of the cardiovascular system was optimized using several optimization algorithms, subject to forward-mode automatic differentiation. Measurement data were synthesized from known parameters to represent the healthy, mitral regurgitant, aortic stenosed and combined valvular disease situations with and without pulmonary hypertension. Eleven model parameters were selected for optimization based on 95 % explained variation in mean pulmonary arterial pressure. A hybrid Adam and limited-memory Broyden-Fletcher-Goldfarb-Shanno optimizer yielded the best results with input data including valvular flow rates, heart chamber volume changes and systematic arterial pressure. Mean absolute percentage errors ranged from 1.8 % to 3.78 % over the simulated test cases. The model was able to capture pressure dynamics under hypertensive conditions with pulmonary arterial systole, diastole, and mean pressure average percentage errors of 1.12 %, 2.49 % and 2.14 %, respectively. The relatively low errors highlight the potential of the proposed model to recover pulmonary pressures for diseased heart valve and pulmonary hypertensive conditions.

Keywords: cardiovascular 0-D model; pulmonary arterial pressure; gradient-based optimization; automatic differentiation

1. Introduction

In sub-Saharan African (SSA) cardiovascular diseases account for approximately 1 million deaths per year [1]. Amongst these, rheumatic heart disease (RHD), ischemic heart disease and pulmonary hypertension (PH) are associated with high mortality rates [2]. RHD in SSA accounts for approximately 23% of worldwide deaths from this disease, where RHD typically results in aortic and mitral valve lesions which leads to valvular regurgitation and/or stenosis. Left untreated, these lesions result in cardiac decompensation through mechanisms of ventricular pressure and volume overload. In rheumatic heart disease, the presence of PH is an independent predictor of mortality [3], therefore, the accurate estimation of PH for RHD cases is crucial for clinical diagnosis and prognostic purposes. The current gold standard for the quantification of pulmonary arterial pressure (PAP) requires the use of invasive right heart catheterization [4] which in developing countries such as SSA, is not readily available, remains costly and is not without risk to the patient [5]. The clinical standard for the non-invasive estimation of PAP utilises transthoracic Doppler echocardiography and associated correlations, but these approaches typically yield inaccurate results [6].

In the present work, a non-invasive computational approach to estimate pulmonary arterial pressure and associated cardiovascular parameters such as pulmonary arterial impedance, left ventricular elastance and systemic venous impedance, is proposed. The

Preprints (www.preprints.org) | NOT PEER-REVIEWED | Posted: 29 August 2022 doi:10.20944/preprints202208.0490.v1

approach utilizes non-invasive measurements including transvalvular flow rates, systemic arterial pressures, and heart volume change over a single heart beat cycle along with scientific machine learning techniques [7]. This, in turn, combines a mechanistic model of the cardiovascular system along with gradient-based optimization and forward-mode automatic differentiation.

Several researchers have recently investigated the efficacy of computational parameter estimation strategies to find unknown physiological parameters of a human cardiovascular system by using clinical measurements, 0-D cardiovascular dynamic models and optimization routines. Bjordalsbakke et al. [8] developed a 0-D computer model of a human systemic loop and used non-invasive measurements and the trust region reflective algorithm to estimate various parameters such as systemic compliances and left ventricle elastance. Synthetic data was generated using the 0-D cardiovascular model with known parameters to gauge the accuracy of the parameter estimation workflow. The mean absolute percentage errors (MAPE) between the true parameters and estimated ones ranged between 1-10%. Kershavarz-Motamed [9] developed a workflow to estimate circulatory parameters using non-invasive measurements such as valvular flow rates measured using Doppler echography and systemic arterial pressures measured using an arm cuff device. The 0-D cardiovascular model was developed using MATLAB Simulink and the parameters optimized using the built-in *fmincon* function. Similarly, Huang and Ying [10] developed an on-line estimation algorithm used to infer the parameters of a 5 component arterial 0-D simulation model. The unknown parameters were estimated by minimizing the squared difference between the model predictions and corresponding measurements, which for this work was generated synthetically using the model and known parameters. The optimization was driven by the use of the *fmincon* function in MATLAB. Colunga et al. [11] used actual invasive and non-invasive patient data to estimate cardiovascular system parameters of a 6 component 0-D model by minimizing the differences between the model predictions and measured data using the Levenberg-Marquardt optimization routine. The workflow was capable of accurately recreating the measured pressure waveforms, but no validation was performed.

To minimize the difference between the 0-D model predictions and the measurements (actual or synthetic) using gradient-based optimization such as Levenberg-Marquardt, a trust region reflective algorithm or MATLAB's *fmincon* requires the calculation of the loss function-parameter gradients. In the discussed research works, the authors applied finite differences [12], [13] to calculate the required gradients. As shown in [14], the use of finite differences leads to computationally expensive and numerically unstable results due to the numerical approximation of the gradients as discussed in [15]. An alternative approach to estimate the gradients is to use automatic differentiation (AD) [15]. AD is able to calculate the analytical gradients using chain rule and computational graphs constructed from the mathematical operations in the computer model. The major limitation of AD is that the 0-D cardiovascular model and differential algebraic equation (DAE) solver should be fully differentiable, meaning the mathematical operations should be tracked and stored to calculate the gradients.

In the present work, a fully differentiable multicompartment cardiovascular 0-D DAE computer model is developed using the *Julia 1.7.0* programming language. The proposed parameter inference model solves the specified set of equations and minimizes the squared differences between the model predictions and non-invasive measurement data by adjusting important cardiovascular parameters. Various optimization algorithms are investigated such as conjugate gradient descent, Adam, and limited-memory Broyden-Fletcher-Goldfarb-Shanno (L-BFGS). The loss function gradients used in the majority of these optimizers are determined using forward-mode automatic differentiation.

The purpose of the present work is to infer the PAP waveforms for healthy cases, mitral regurgitation and aortic valve stenosis cases, using synthetic non-invasive data generated using known parameters and the 0-D model. In addition, to determine the reduced set of parameters which have a significant effect on the mean PAP, a local sensitivity analysis is performed. To the best of the authors' knowledge, this is the first work that

Preprints (www.preprints.org) | NOT PEER-REVIEWED | Posted: 29 August 2022 doi:10.20944/preprints202208.0490.v1

directly investigates the ability of a scientific machine learning model to infer PAP values using non-invasive, clinically available measurements and a 0-D cardiovascular system model accounting for the dynamics of the heart valves. To lower costs of deploying the proposed algorithm and to enable reproducibility, the computer models are developed in free and opensource *Julia* libraries namely *DifferentialEquations.jl* [16], *ForwardDiff.jl* [17] (automatic differentiation), *Optim.jl* [18] (optimization framework) and *Flux.jl* [19] (first-order gradient-descent optimizers).

2. Materials and Methods

Figure 1 below depicts the parameter inference model workflow. The model starts by initializing the unknown cardiovascular model parameters θ such as left ventricle (LV) elastance, pulmonary arterial resistance and systemic venous impedance; it should be noted that only the model parameters that have a significant effect on the mean PAP will be optimized as will be discussed in Section 2.3. Once initialized, the important model parameters are used to simulate a single cardiac cycle using a fully differentiable 0-D cardiovascular system model $H(\theta)$. Next the model predictions $\hat{X}$ corresponding to the available non-invasive measurements $\tilde{X}$ are extracted. The extracted model predictions along with the synthetic non-invasive measurements are then fed to a loss function $L(\hat{X}, \tilde{X})$ which calculates the sum-squared difference. If the loss function is above the prescribed convergence criteria ε, the model then calculates the loss function gradients using forward-mode automatic differentiation and then adjusts the parameters using this information and the process is then repeated. In the subsections below more information relating to the 0-D model, datasets, optimization parameters and optimizers will be provided.

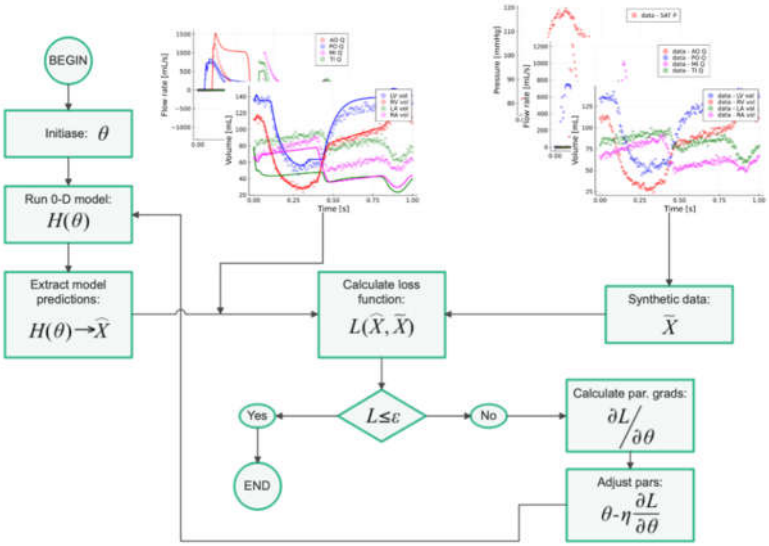

Figure 1. Computer model flowchart.

2.1. Mechanistic Model of Cardiovascular System

Central to the pulmonary inference computer model (shown in Figure 1) is the 0-D DAE model of the human cardiovascular system. In the current work a multi-compartment model including the four heart chambers, corresponding heart valves, pulmonary loop and systemic loop is developed. A layout of the cardiovascular network model is shown in Figure 2. The model is based on the work of Korakianitis and Shi [20].

Preprints (www.preprints.org) | NOT PEER-REVIEWED | Posted: 29 August 2022 doi:10.20944/preprints202208.0490.v1

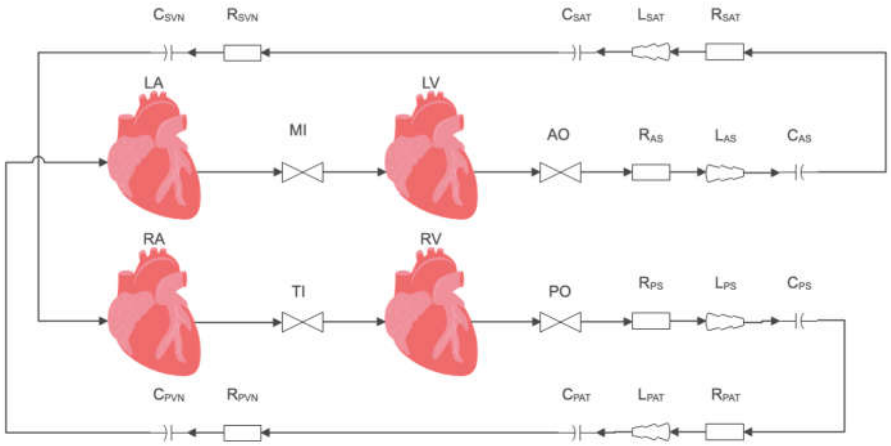

Figure 2. 0-D cardiovascular network model layout. Aortic – AO, mitral – MI, pulmonary – PO, tricuspid – TI, aortic sinus – AS, systemic arteries – SAT, systemic veins – SVN, pulmonary sinus – PS, pulmonary arteries – PAT, pulmonary veins – PVN.

To simulate the pressure and volume changes of the heart chambers the mathematical model of Suga et al. [21] was applied as seen in Equation (1), where $P_{LV}(t)\ [mmHg]$ is the LV pressure at time t, $P_{LV,0}$ is the unstressed LV pressure (set to a value of 1 one for all heart chambers [22]), $e_{LV}(t)\ [s]$ is the LV time-varying elastance function, $V_{LV}(t)[mL]$ is the instantaneous LV volume and $V_{LV,0}$ is the unstressed LV volume.

$$P_{LV}(\mathrm{t}) = P_{LV,0} + e_{LV}(t)\left(V_{LV}(t) - V_{LV,0}\right) \tag{1}$$

To simulate the changes in ventricle blood volume the mass conservation equation for an incompressible fluid can be applied to the ventricle control volume yielding a set of ODEs for each heart chamber. The change in ventricle blood volume for the LV is shown in Equation (2), where $Q_{MI}(t)$ and $Q_{AO}(t)$ are the mitral and aortic valve volume flow rates at time step t.

$$\frac{dV_{LV}}{dt} = Q_{MI}(t) - Q_{AO}(t) \tag{2}$$

The time-dependent elastance function for the LV is calculated using Equation 3, where $E_{LV,s}\ [{}^{mmHg}/_{mL}]$ is the LV systolic elastance and $E_{LV,d}$ is the diastolic ventricular elastance. A similar equation is used to predict the changes in right ventricle (RV) elastance.

$$e_{LV}(t) = E_{LV,d} + \frac{E_{LV,s} - E_{LV,d}}{2} f(t) \tag{3}$$

The ventricular activation function used to simulate the heart muscle contraction and relaxation was taken from the work of Bozkurt [23], and is shown in Equation (4).

$$f(t) = \begin{cases} 1 - cos\left(\dfrac{t}{T_1}\pi\right) & if\ 0 \le t < T_1 \\ 1 + cos\left(\dfrac{t - T_1}{T_2 - T_1}\pi\right) & if\ T_1 \le t < T_2 \\ 0 & if\ T_2 \le t < T \end{cases} \tag{4}$$

In Equation (4), the end time of systole is set to $T_1 = 0.3\,T\ [s]$ and the end time of ventricular relaxation is set to $T_2 = 0.45\,T$ [23] where T is the heartbeat period which in the present work was fixed to a value of $1\ [s]$. The RV is simulated also using Equation (1)–(4) but with corresponding RV parameters (Table 1).

To simulate the left and right atrium (LA and RA) pressure and blood volume changes, Equations (1)–(2) are used similarly to the ventricle calculations but with corresponding atrium parameters as seen in Table 1. The time-dependent elastance of the left atrium is calculated as seen in Equation (5), where $E_{LA,min}$ and $E_{LA,max}$ are the minimal and maximal LA elastances, and $f_a(t)$ is the atrial contractility activation function.

Preprints (www.preprints.org) | NOT PEER-REVIEWED | Posted: 29 August 2022 doi:10.20944/preprints202208.0490.v1

$$e_{LA}(t) = E_{LA,min} + \frac{E_{LA,max} - E_{LA,min}}{2} f_a(t - D) \quad (5)$$

The atrial contractility activation function is in turn calculated using Equation (6), where $D = 0.04\ [s]$ is the time of atrial relaxation.

$$f_a(t) = \begin{cases} 0 & if\ 0 \le t < T_a \\ 1 - cos\left(2\pi \frac{t - T_a}{T - T_a}\right) & if\ T_a \le t < T \end{cases} \quad (6)$$

In Equation (6), $T_a = 0.8\,T$ is the time at onset of atrial contraction. Table 1 below contains the cardiovascular parameters used in the heart chamber models.

Table 1. Heart model nominal parameters (values in parenthesis indicate upper and lower boundaries for sensitivity analysis and normalization) [20].

Parameters	Left Heart	Right Heart
	Atriums	
$E_{LA,max}, E_{RA,max}$	0.25 (0.0, 1.0)	0.25 (0.0, 1.0)
$E_{LA,min}, E_{RA,min}$	0.15 (0.0, 0.5)	0.15 (0.0, 0.5)
$V_{LA,0}, V_{RA,0}$	4.0 (1.0, 20.0)	4.0 (1.0, 10.0)
	Ventricles	
$E_{LV,s}, E_{RV,s}$	2.5 (0.5, 5.0)	1.15 (0.5, 5.0)
$E_{LV,d}, E_{RV,d}$	0.1 (0.0, 1.0)	0.1 (0.0, 0.5)
$V_{LV,0}, V_{RV,0}$	5.0 (1.0, 20.0)	10.0 (1.0, 50.0)

To estimate the blood flow rate through each of the four heart valves pressure gradient across the heart valve and the valve opening area is used as seen in Equation (7), where $i = AO, PO, TI, MI$. In Equation (7), CQ is the valvular flow coefficient which is set to 400 $\left[\frac{mL}{s\ mmHg^{0.5}}\right]$ for the atrioventricular valves and 350 $\left[\frac{mL}{s\ mmHg^{0.5}}\right]$ for the semilunar valves [22].

$$Q_i = CQ \cdot A_r(t)\sqrt{\Delta P(t)} \quad (7)$$

In the previous equation, the pressure gradient across the valve $\Delta P(t)$ is calculated using Equation (8), where $P_{in}(t)$ is the valve upstream static pressure and $P_{ex}(t)$ is the valve downstream pressure. For example, the aortic valve inlet pressure would be the LV pressure $P_{LV}(t)$ and the exit pressure the aortic sinus pressure $P_{AS}(t)$ as shown in Figure 2.

$$\Delta P(t) = \begin{cases} P_{in}(t) - P_{ex}(t) & if\ P_{in} \ge P_{ex} \\ P_{ex}(t) - P_{in}(t) & if\ P_{ex} > P_{in} \end{cases} \quad (8)$$

In Equation (7), $A_r(t)$ is the area opening ratio of the heart valve and is defined as the fraction of flow area at a given time step divided by the area of the valve when fully open. For the present work, the valve opening fraction is calculated as a function of the valve opening angle β_v as shown in Equation (9), where $\beta_{v,max}$ is the maximum opening angle of the valve cusps.

$$A_r(t) = \frac{(1 - cos[\beta_v(t)])^2}{(1 - cos[\beta_{v,max}])^2} \quad (9)$$

To estimate the time-dependent valve opening angle for each heart valve, the angular momentum equation is solved as shown in Equation (10).

$$\frac{d^2\beta_v}{dt^2} = [P_{in}(t) - P_{ex}(t)] \cdot K_p cos(\beta_v) \quad (10)$$

The valvular force coefficient K_p $\left[\frac{mmHg \cdot s^2}{mL}\right]$ was set to a constant value of 5500 for all valves as recommended by [20].

The systemic and pulmonary vasculature are modelled using the electro-hydraulic analogue equations for fluid flow in a 0-D network. Each loop is modelled using 5 components that consist of inductive, capacitive, and resistive components as seen in Figure

Preprints (www.preprints.org) | NOT PEER-REVIEWED | Posted: 29 August 2022 doi:10.20944/preprints202208.0490.v1

2. For the sake of brevity only the systemic loop equations will be provided; for more detail on the model equations, please see [24]. The flow rate through the aortic sinus and associated sinus inlet pressure are calculated using the following ODEs.

$$L_{AS}\frac{dQ_{AS}}{dt} = (P_{AS} - P_{SAT}) - R_{AS}Q_{AS} \tag{11}$$

$$C_{AS}\frac{dP_{AS}}{dt} = Q_{AO} - Q_{AS} \tag{12}$$

In Equations (11) and (12), L_{AS} $\left[\frac{mmHg\cdot s^2}{mL}\right]$ is the blood flow inertia through the sinus, Q_{AS} is the volume flow rate of blood through the sinus, P_{AS} is the inlet sinus static pressure, P_{SAT} is the arterial inlet pressure, R_{AS} $\left[\frac{mmHg\cdot s}{mL}\right]$ is the sinus flow resistance and C_{AS} $\left[\frac{mL}{mmHg}\right]$ is the sinus compliance. The arterial pressure and volume flow rate is simulated using Equations (13) and (14).

$$L_{SAT}\frac{dQ_{SAT}}{dt} = (P_{SAT} - P_{SVN}) - R_{SAT}Q_{SAT} \tag{13}$$

$$C_{SAT}\frac{dP_{SAT}}{dt} = Q_{AS} - Q_{SAT} \tag{14}$$

The inlet venous pressure is calculated using Equation (15) and the venous flow rate using Equation (16).

$$C_{SVN}\frac{dP_{SVN}}{dt} = Q_{SAT} - Q_{SVN} \tag{15}$$

$$Q_{SVN}R_{SVN} = P_{SVN} - P_{RA} \tag{16}$$

The vasculature parameters such as resistance and capacitance for the systemic and pulmonary loops can be found in Table 2.

Table 2. Systemic and pulmonary loop parameters (values in parenthesis is used for upper and lower boundaries).

Compartment	Resistance $\left[\frac{mmHg\cdot s^2}{mL}\right]$	Inductance $\left[\frac{mmHg\cdot s}{mL}\right]$	Capacitance $\left[\frac{mL}{mmHg}\right]$
	Systemic loop		
AS	0.003 (0.0003, 0.03)	0.000062 (1E-4, 1E-3)	0.08 (0.008, 0.8)
SAT	0.05 (0.005, 1.0)	0.0017 (1.7E-3, 0.017)	1.6 (0.16, 3.2)
SVN	0.075 (0.0075, 0.75)	0	20.5 (5.0, 50.0)
	Pulmonary loop		
PS	0.002 (2E-3, 2E-2)	0.000052 (1E-4, 1E-3)	0.18 (0.018, 2.0)
PAT	0.05 (0.001, 0.1)	0.0017 (1.7E-3, 0.017)	3.8 (0.38, 6.0)
PVN	0.006 (6E-4, 0.01)	0	20.5 (5.0, 50.0)

To solve the above mentioned DAEs of the cardiovascular system the explicit Runge-Kutta solver with the Bogacki-Shampine 3/2 method is applied. The solver's relative and absolute tolerances are set to 1E-4 and 1E-6 respectively and the maximum allowable iterations per time step was set to 1E6. To numerically integrate the DAEs, certain physical constraints must be enforced on the dynamic valve model. To incorporate the discontinuities which results from the valve motion limits (fully open or closed) the following conditions are included in the simulation procedure for each valve.

$$\beta_v = \begin{cases} \beta_v = \beta_{v,max}, \ \dfrac{d\beta_v}{dt} = 0 \ if \ \beta_v \geq \beta_{v,max} \\ \beta_v = \beta_{v,min}, \ \dfrac{d\beta_v}{dt} = 0 \ if \ \beta_v \leq \beta_{v,min} \\ \beta_v \ if \ \beta_{v,min} < \beta_v < \beta_{v,max} \end{cases} \tag{17}$$

Preprints (www.preprints.org) | NOT PEER-REVIEWED | Posted: 29 August 2022 doi:10.20944/preprints202208.0490.v1

2.2. Data and Measurements

In the present work, synthetic data is generated using the 0-D cardiovascular model and used as pseudo clinical measurements. The benefit of this approach is that the true underlying parameters being optimized is known and the obvious disadvantage is that one assumes the model is capable of capturing the dynamics of an actual cardiovascular system. Nonetheless, other published authors have also followed this approach [8].

In the current work, two datasets are used as synthetic measurements. The first dataset, namely D1, contains the transvalvular flow rates $Q_{AO}, Q_{PO}, Q_{TI}, Q_{MI}$ and the systemic arterial pressure P_{SAT} for a single cardiac cycle. The second dataset, D2, additionally contains the heart chamber volume changes, $V_{LV}, V_{RV}, V_{LA}, V_{RA}$. The motivation for using two datasets is to investigate the effect of additional non-invasive data on the model parameter inference accuracy as will be discussed in Section 3.2.

For each dataset generation run the ODE integrator solves for multitudes of time steps dictated by the numerical integrator accuracy control, but to replicate actual use of the model, only $N = 200$ samples are stored and used during the parameter optimization phase. Additionally, noise is added to the pseudo-measurement results. The standard deviation used for the normally distributed noise generation of the chamber volumes and flow rates were set to 3% of the respective mean values and for the arterial pressure the standard deviation was set to 1% of the mean simulated arterial pressure value. Figure 3 below shows an example of the pseudo-measurements used for the healthy non-hypertensive conditions.

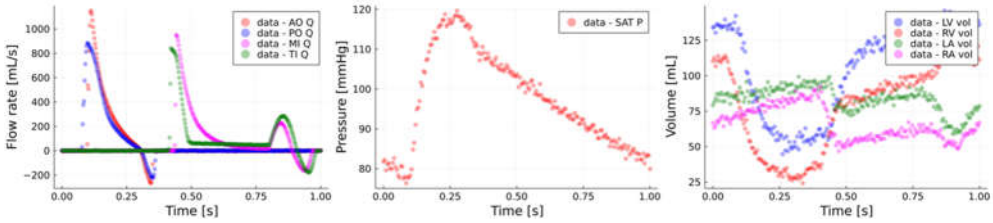

Figure 3. Pseudo-measurements.

To clinically measure the data shown in Figure 3, different equipment can be utilized. For the present work, the following clinical measurements are proposed for further retrospective clinical studies. The brachial arterial pressure can be measured continuously using a CNAP monitor and volume clamp method as discussed by [25]. The transvalvular flow rates should be measured using Doppler echocardiography and the heart chamber volumes using either 3D magnetic resonance imaging (MRI) or Doppler echocardiography.

To simulate the 0-D cardiovascular model and solve for the model dependent variables such as systemic arterial pressure (Equation (14)) and aortic sinus flow rate (Equation (11)) requires the initial conditions to be known. The initial conditions vector is shown in Equation (18).

$$\hat{X}_{init} = \left[V_{LV}^{init}, V_{LA}^{init}, P_{AS}^{init}, Q_{AS}^{init}, P_{SAT}^{init}, Q_{SAT}^{init}, P_{SVN}^{init}, V_{RV}^{init}, V_{RA}^{init}, P_{PS}^{init}, Q_{PS}^{init}, P_{PAT}^{init}, Q_{PAT}^{init}, P_{PVN}^{init}\right] \quad (18)$$

In a clinical application of the proposed parameter inference model, these initial conditions should be extracted from the available non-invasive measurements. The initial transvalvular flow rates and heart chamber volumes can directly be taken as the initial entries in D1 and D2 for the respectively data streams. Similarly, the initial cycle systemic arterial pressure can be extracted from D1 and D2 and in the present work it is assumed that the initial aortic sinus pressure is equal to the initial systemic arterial pressure. The initial systemic and pulmonary arterial flow rates are approximated using Equations (19) and (20), where SV_{LV} and SV_{RV} are the left and right ventricular stroke volumes which can be non-invasively estimated using Doppler echography.

Preprints (www.preprints.org) | NOT PEER-REVIEWED | Posted: 29 August 2022 doi:10.20944/preprints202208.0490.v1

$$Q_{SAT}^{init} = \frac{SV_{LV}}{T} \tag{19}$$

$$Q_{PAT}^{init} = \frac{SV_{RV}}{T} \tag{20}$$

The remaining initial conditions, namely P_{SVN}^{init}, P_{PVN}^{init}, P_{PS}^{init} and P_{PAT}^{init}, are difficult to accurately measure non-invasively and, therefore, these parameters are optimized in conjunction with selected important model parameters (Tables 1 and 2) which significantly affect mean pulmonary arterial pressure, as will be discussed in Section 2.3.

2.3. Local Sensitivity Analysis

A local sensitivity analysis is performed using the 0-D cardiovascular model to identify model parameters (Tables 1 and 2) which has a significant effect on the mean PAP. These identified parameters are then used in the optimization phase of the present work to infer the PAP waveform and estimate the true cardiovascular parameters.

To find these important parameters the sensitivity percentages of each parameter, (designated $SP_{PAP,i}$ for the i^{th} parameter) are calculated as seen in Equation (21). The top parameters that make up 95% of the variations in mean PAP are then selected as the important parameters to be optimized.

$$SP_{PAP,i} = 100\% \cdot \frac{SI_{PAP,i}}{\sum_{j=1}^{n_{tot}} SI_{PAP,j}} \tag{21}$$

In Equation (21), $SI_{PAP,i}$ is the i^{th} parameter sensitivity index which is calculated using Equation (22). To estimate the required gradients of the mean PAP, forward-mode AD is utilized. Forward-mode AD is capable of traversing any native *Julia* code, therefore, is able to differentiate through the ODE integrator solution, to calculate the required gradients in a computationally efficient manner [17]. The gradients are calculated around the nominal values shown in Tables 1 and 2 but seeing as the model parameters vary in orders of magnitude and units, each mean PAP gradient is multiplied by the difference between the upper $\theta_{i,ub}$ and lower $\theta_{i,lb}$ parameter boundaries to normalize the calculated parameter gradients.

$$SI_{PAP,i} = \left| \frac{\partial \left(\frac{1}{N_t^*} \sum_{j=1}^{N_t^*} P_{PAP}^j \right)}{\partial \theta_i} \right| \cdot \left(\theta_{i,ub} - \theta_{i,lb} \right) \tag{22}$$

2.4 Parameter Optimization

To estimate θ which minimizes the difference between the 0-D model predictions and the synthetic (pseudo) measurements in the present work, the sum-squared error (SSE) loss function is minimized using selected optimizers. The SSE for the j^{th} measurement (e.g., LV volume, systemic arterial pressure, or mitral valve flow rate) is calculated using Equation (23).

$$J(\hat{x}_j, \tilde{x}_j) = \left(\sum_{i=1}^{N} \left(\hat{x}_j^i(\bar{\theta}) - \tilde{x}_j^i \right)^2 \right)_j \tag{23}$$

In Equation (23), $\hat{x}_j^i$ is the j^{th} simulation output at time step i and $\tilde{x}_j^i$ is the j^{th} synthetically measured value (e.g., arterial pressure or LV volume) at time step i. Further, $\bar{\theta}$ is the parameter vector containing all the selected important parameters, $\hat{x}_j$ is the vector of model predictions for measurement j and $\tilde{x}_j$ is the vector of synthetic measurements for measurement j. The loss function minimized by the computer model is then simply the summation of the different measurement losses $J(\hat{x}_j, \tilde{x}_j)$ as seen in Equation (24), where d is the number of measurement streams (5 and 9 for D1 and D2 respectively, as mentioned in Section 2.2).

Preprints (www.preprints.org) | NOT PEER-REVIEWED | Posted: 29 August 2022 doi:10.20944/preprints202208.0490.v1

$$L(\hat{X}(\bar{\theta}), \tilde{X}) = \sum_{i=1}^{d} \left(J(\hat{x}_i, \tilde{x}_i) \right) \tag{23}$$

To speed up optimization convergence the parameter and measurement datasets were normalized using min-max scaling. For the parameter vector the upper and lower boundaries listed in Tables 1 and 2 were used. The measurements and model predictions were scaled using the maximum and minimum measured values, e.g., for parameter i, $\max(\tilde{x}_i)$ and $\min(\tilde{x}_i)$.

In the present work, three optimization strategies are employed. The first uses the adaptive moment estimation (Adam) first-order optimizer. The Adam algorithm is shown in Equation (24) below.

$$\begin{gathered} \bar{m} \leftarrow \beta_1 \bar{m} + (1 - \beta_1) \nabla_\theta L(\bar{\theta}) \\ \bar{s} \leftarrow \beta_1 \bar{s} + (1 - \beta_2) \nabla_\theta C(\bar{\theta}) \otimes \nabla_\theta L(\bar{\theta}) \\ \bar{m} \leftarrow \frac{\bar{m}}{1 - \beta_1^t} \\ \bar{s} \leftarrow \frac{\bar{s}}{1 - \beta_2^t} \\ \bar{\theta}^{new} \leftarrow \bar{\theta} - \eta \bar{m} \otimes \sqrt{(\bar{s} + \epsilon)^{-1}} \end{gathered} \tag{24}$$

The scaling $\bar{s}$ and momentum $\bar{m}$ matrices are initialized to 0 at the start of the Adam training algorithm, t is the iteration counter, $\epsilon = 1 \cdot 10^{-8}$ is the smoothing term, β_1 is the momentum decay hyperparameter and is set to 0.9 and β_2 is the scaling hyperparameter and is set to 0.999. In Equation (24), $\nabla_\theta L(\bar{\theta})$ are the gradients of the cost function with respect to the optimization parameters. For the optimization runs, the learning rate parameter η is fixed to a value of 0.005.

The second strategy uses the conjugate gradient descent [26] optimizer to minimize the loss function. The conjugate gradient optimizer update algorithm for the parameters is shown in Equation (25).

$$\begin{gathered} \bar{\theta}^{new} \leftarrow \bar{\theta} - \eta \bar{d}^{new} \\ \bar{d}^{new} \longleftarrow \nabla_\theta L(\bar{\theta}) \; - \; \gamma^{new} \bar{d}^{old} \end{gathered} \tag{25}$$

For the first iteration, $\bar{d} = \nabla_\theta L(\bar{\theta})$. In the present work, the learning rate parameter η is estimated per iteration using the line search proposed by Hager and Zhang [27]. The scalar variable γ^{new} is also calculated using the method proposed by Hager and Zhang.

The third strategy applies a combination of Adam and L-BFGS [28] optimizers to minimize the loss function. For this strategy, the first 50 iterations of the optimization phase were completed using Adam, after which the model switches over to the L-BFGS. The interested reader can see [26] for more information about the L-BFGS optimization algorithm.

3. Results

To find the best optimization strategy and to demonstrate the ability of the proposed method to infer the PAP waveforms for diseased heart valve cases, two investigations were performed. The first looks at the effect of selected optimizers and dataset contents on the parameter estimation accuracy and pulmonary pressures for healthy heart valves. Using the best-performing optimizer of this study, the work then investigates the capability of the model to capture the PAP waveforms for synthetic data generated with induced mitral regurgitation and aortic stenosis with and without increased pulmonary arterial impedance.

3.1. Local Sensitivity Analysis

Before the two above sets of results are discussed, the important model parameters selected using the local sensitivity analysis will be provided. Figure 4 shows a histogram

Preprints (www.preprints.org) | NOT PEER-REVIEWED | Posted: 29 August 2022 doi:10.20944/preprints202208.0490.v1

of all the model parameters and their respective sensitivity percentages as calculated using Equation (21).

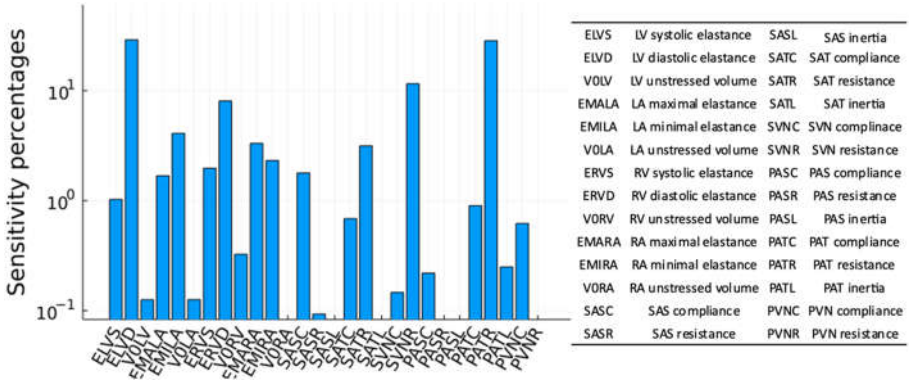

ELVS	LV systolic elastance	SASL	SAS inertia
ELVD	LV diastolic elastance	SATC	SAT compliance
V0LV	LV unstressed volume	SATR	SAT resistance
EMALA	LA maximal elastance	SATL	SAT inertia
EMILA	LA minimal elastance	SVNC	SVN complinace
V0LA	LA unstressed volume	SVNR	SVN resistance
ERVS	RV systolic elastance	PASC	PAS compliance
ERVD	RV diastolic elastance	PASR	PAS resistance
V0RV	RV unstressed volume	PASL	PAS inertia
EMARA	RA maximal elastance	PATC	PAT compliance
EMIRA	RA minimal elastance	PATR	PAT resistance
V0RA	RA unstressed volume	PATL	PAT inertia
SASC	SAS compliance	PVNC	PVN compliance
SASR	SAS resistance	PVNR	PVN resistance

Figure 4. Model parameter sensitivity percentages.

From the results it is seen that the parameter with the largest effect on the mean PAP is the pulmonary arterial resistance (28.8%), followed by the left ventricular diastolic elastance (28.1%), systemic venous resistance (12%) and the right ventricular diastolic elastance (8.3%). In total, 11 parameters were selected to be optimized in subsequent sections along with the mentioned initial conditions (Section 2.2). Equation (26) below shows the important parameter vector.

$$\bar{\theta} = [\, R_{PAT}\ E_{LV,d}\ R_{SVN}\ E_{RV,d}\ E_{LA,min}\ E_{RA,max}\ R_{SAT}\ E_{RA,min}\ E_{RV,s}\ E_{LA,max}\ E_{LV,s}\ P_{PVN}^{init}\ P_{SVN}^{init}\ P_{AS}^{init}\ P_{PAT}^{init}\,] \tag{26}$$

The local sensitivity analysis was also performed for both diseased heart valve conditions and the analysis identified the same parameters as shown in Equation (26), but with differences in the sensitivity percentages allocated to each parameter.

3.2. Healthy Cardiovascular System Results

Using the nominal model parameters shown in Tables 1 and 2 synthetic datasets (D1 and D2) are generated and used as pseudo measurements. The proposed inference model is tasked to recover the important model parameters (Equation (26)) while the remaining parameters are fixed to their respective nominal values. The goal of this investigation is to quantify the effect of the addition of heart chamber volume data and optimizer selection on parameter inference and pulmonary waveform prediction accuracy.

To estimate the parameter inference errors the absolute percentage error (APE) metric is used. The equation used to calculate the APE for the i^{th} important parameter is shown in Equation (27).

$$APE = 100\% \cdot \frac{|\theta_i - \theta_{i,true}|}{\theta_{i,true}} \tag{27}$$

Table 3 below contains the APEs calculated for the different important parameters using the different datasets and optimizers. Additionally, the mean APE (MAPE), is also provided. The results indicate that the addition of the heart chamber volume data (D2) significantly improves the inference accuracy for all the applied optimizers. Studying Equation (2) and Figure 2 it becomes clear that the heart chamber volume trends indirectly contain information about the atria upstream flow rates (Q_{svn} *and* Q_{pvn}), which is needed to integrate the mass continuity equation to find the time-dependent changes in chamber volume. The indirect addition of these flow rates seems to positively impact the ability of the inference model to accurately predict the unknown model parameters.

Preprints (www.preprints.org) | NOT PEER-REVIEWED | Posted: 29 August 2022 doi:10.20944/preprints202208.0490.v1

Table 3. Absolute percentage errors per parameter for datasets generated using nominal model parameters.

Parameters	SP	D1 + ADAM	D1 + CGD	D1 + L-BFGS (Hybrid)	D2 + ADAM	D2 + CGD	D2 + L-BFGS (Hybrid)
$E_{LV,s}$	1,42	7,1	3,2	8,8	0,4	1,7	2,1
$E_{LV,d}$	28,18	10,3	9,9	3,4	2,0	2,0	1,3
$E_{LA,max}$	1,62	155,7	141,7	109,6	5,3	4,3	1,3
$E_{LA,min}$	4,11	89,3	86,3	64,1	5,8	3,8	1,9
$E_{RV,s}$	2,04	1,9	1,4	0,2	1,0	2,0	0,8
$E_{RV,d}$	8,33	12,8	29,9	26,7	1,9	2,6	2,1
$E_{RA,max}$	3,43	22,1	46,5	41,3	1,8	2,4	0,9
$E_{RA,min}$	2,39	12,4	14,0	13,9	1,7	1,4	2,3
R_{SAT}	3,17	8,5	6,7	7,1	4,3	2,1	0,3
R_{SVN}	11,95	20,6	10,3	18,6	14,3	14,7	12,6
R_{PAT}	28,83	5,0	39,0	2,9	2,7	3,8	3,0
P_{PVN}^{init}	-	3,8	23,8	17,4	4,4	6,3	8,0
P_{SVN}^{init}	-	14,1	2,5	12,4	2,1	8,2	0,9
$P_{PS}^{init}, P_{PAT}^{init}$	-	5,4	16,6	15,3	0,0	1,2	1,4
MAPE	-	26,4	30,8	24,4	3,4	4,0	2,8

Of the three model configurations trained using D2, the Adam-L-BFGS hybrid optimization approach resulted in the lowest overall MAPE, followed by the Adam optimization approach. For the hybrid optimization approach all parameters had APEs between 0-5% except the systemic venous resistance and the initial pulmonary venous pressure parameters. Although these two parameter inference errors are relatively high, they have a small effect on the ability of the model to accurately recover important PAP values, as seen in Table 4. It is interesting to note that the Adam optimization approach more accurately predicts the pulmonary pressures but has a higher overall MAPE compared to the hybrid optimization approach. A possible explanation of this is that the estimated pulmonary arterial resistance parameter has a lower APE for the Adam approach when compared to the value predicted using the hybrid optimizer approach. Nonetheless, seeing as the hybrid optimizer produces the most accurate parameter estimates, it was selected for further studies involving diseased mitral and aortic heart valves.

Table 4. Pulmonary pressure predictions for nominal model parameters.

PAP	True Values	D2 + ADAM	D2 + L-BFGS (Hybrid)
Diastole	13,93	13,96	13,94
Systole	25,11	25,05	24,96
Mean	17,65	17,58	17,42

3.3. Diseased Heart Valve Case Studies

To investigate the ability of the proposed model to infer model parameters and PAP values for diseased heart valve cases, additional datasets were generated. These datasets consisted of data generated for induced aortic stenosis, mitral regurgitation, and a combination of these two valve diseases. To simulate aortic stenosis the maximal valve opening angle is limited to 49.4° which corresponds to a valvular flow area of 1 [cm²] for a valve diameter of 24.7 mm. Mitral regurgitation is induced by limiting the minimal mitral valve closing angle to 33°, which corresponds to an open flow area fraction of 5%. For the combined case, both the aortic stenosis and mitral regurgitation limits are induced simultaneously.

For the three valvular disease cases, the nominal parameters listed in Tables 1 and 2 were used to generate synthetic data. The APEs calculated for the five parameters with the highest SP values can be found in Table 5 along with MAPEs calculated using all the parameters and initial conditions. The MAPE results show that the selected approach

Preprints (www.preprints.org) | NOT PEER-REVIEWED | Posted: 29 August 2022 doi:10.20944/preprints202208.0490.v1

using D2, and the hybrid optimizer is capable of predicting the unknown model parameters for the three diseased cases with the same relative accuracy compared to the MAPE value calculated for the healthy case (Table 3). The case with the highest MAPE and highest parameter APE ($R_{SVN} = 12.12\%$) is the mitral regurgitation case, whereas the results show that the inclusion of aortic stenosis decreases the predicted parameter errors.

Table 5. Absolute percentage errors per parameter for datasets generated using nominal model parameters with aortic stenosis, mitral regurgitation and both valvular diseases present.

Parameters	Aortic stenosis	Mitral regurgitation	Combined
$E_{LV,d}$	1,26	0,62	1,93
$E_{LA,min}$	1,44	0,74	1,82
$E_{RV,d}$	0,05	1,87	2,03
R_{SVN}	0,39	12,12	7,14
R_{PAT}	2,80	7,74	6,62
MAPE (all parameters)	1,70	3,78	3,33

Figure 5 shows the right ventricle and pulmonary arterial pressure waveforms simulated using the predicted model parameters for the different diseased heart valve cases. Additionally, the systole, diastole and mean PAP predicted, and true values are also included in Figure 5, where the true values are the pressure values with no noise present. The results show that using the inferred model parameters, the 0-D cardiovascular model can with relative accuracy capture the true waveforms generated with the nominal parameter set for both the unobserved ventricle and pulmonary artery pressures. For the combined diseased case, it is seen that the model using the inferred parameters slightly underpredicts the average pulmonary pressure prediction (average calculated using mean, systole and diastole values) by approximately 1.5%, whereas for the other cases the model can accurately capture the diastole, systole, and mean PAP values.

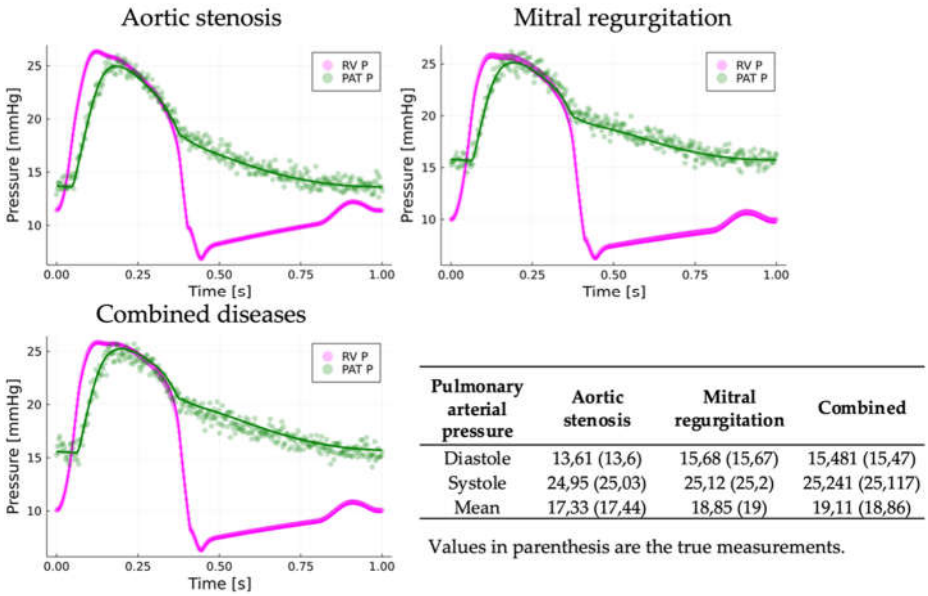

Pulmonary arterial pressure	Aortic stenosis	Mitral regurgitation	Combined
Diastole	13,61 (13,6)	15,68 (15,67)	15,481 (15,47)
Systole	24,95 (25,03)	25,12 (25,2)	25,241 (25,117)
Mean	17,33 (17,44)	18,85 (19)	19,11 (18,86)

Values in parenthesis are the true measurements.

Figure 5. Pulmonary arterial and right ventricle pressure waveforms predicted by model along with predicted important PAP values using nominal model parameters. Solid lines - predicted values; markers – actual waveforms + noise.

As seen in the results in Figure 5, the mean PAP values for the different cases are below 25 mmHg [5], which is the typical upper limit for normal pulmonary pressures. To induce pulmonary hypertension the pulmonary resistance was increased from 0.05 to 0.25 $\left[\frac{mmHg \cdot s^2}{mL}\right]$ and the synthetic data regenerated (transvalvular flow rates, heart chamber volumes and systemic arterial pressures) for the mentioned diseased heart valve settings.

Preprints (www.preprints.org) | NOT PEER-REVIEWED | Posted: 29 August 2022 doi:10.20944/preprints202208.0490.v1

Using these new datasets, the inference model was again applied to recover the unknown model parameters, the goal being to investigate the model accuracy for hypertensive conditions. Table 6 contains the top 5 important parameter APEs along with the MAPE using all the predicted parameters. The results again indicated that the inference model can, with relative accuracy, find the unknown important parameter values and the effect of increased pulmonary arterial resistance is not substantial on the overall MAPE values. That being said, it is interesting to notice that the pulmonary arterial resistance APEs from Table 6 are on average approximately 3.5% higher when compared to the values in Table 5 where the nominal resistance value is used for pseudo-measurement generation.

Table 6. Absolute percentage errors per parameter for datasets generated using increased pulmonary arterial resistance with aortic stenosis, mitral regurgitation and both valvular diseases present.

Parameters	Aortic stenosis	Mitral regurgitation	Combined
$E_{LV,d}$	1,63	0,76	0,58
$E_{LA,min}$	1,80	1,23	0,79
$E_{RV,d}$	4,29	0,52	0,80
R_{SVN}	0,07	2,58	5,06
R_{PAT}	6,72	4,95	10,39
MAPE (all parameters)	3,13	2,51	3,42

Figure 6 shows the pulmonary arterial and right ventricular pressure waveforms along with the predicted and actual PAP values. These results show that although the prediction APEs for R_{PAT} are higher for the increased resistance cases, the inference model is still capable of capturing the pulmonary pressure dynamics with relative accuracy. However, for the combined case, it is noted that the model slightly under predicts the systolic right ventricular pressure, due to the overprediction of the right ventricular systolic elastance parameter (1.21 mmHg/mL vs. 1.15 mmHg/mL) which lowers pressure generation in the ventricle.

For the PAP systole, diastole and mean values, the inference model has average error percentages of 1.12%, 2.49% and 2.14% respectively. These relatively low errors highlight the possible ability of the proposed model to capture pulmonary pressures for diseased heart valve and hypertensive conditions.

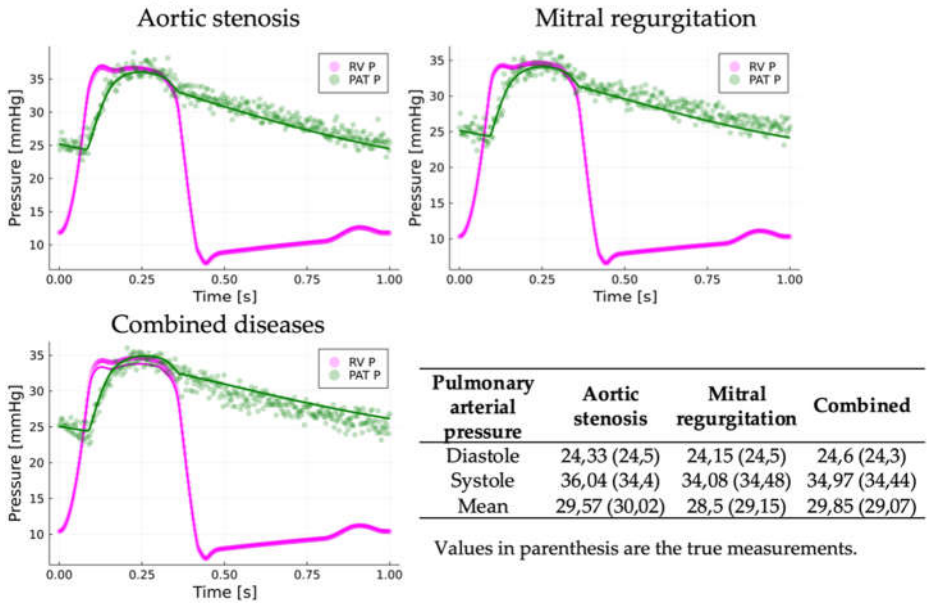

Pulmonary arterial pressure	Aortic stenosis	Mitral regurgitation	Combined
Diastole	24,33 (24,5)	24,15 (24,5)	24,6 (24,3)
Systole	36,04 (34,4)	34,08 (34,48)	34,97 (34,44)
Mean	29,57 (30,02)	28,5 (29,15)	29,85 (29,07)

Values in parenthesis are the true measurements.

Figure 5. Pulmonary arterial and right ventricle pressure waveforms predicted by model along with predicted important PAP values using increased pulmonary arterial resistance. Solid lines - predicted values; markers – actual waveforms + noise.

5. Conclusions

In the present work it was demonstrated that the proposed algorithm can successfully recover the pulmonary arterial pressure waveform and associated clinically important values (systolic, diastolic, and mean values) using non-invasive measurements and a 0-D cardiovascular dynamic network model. It was found that using transvalvular flow rates, heart chamber volumes and systemic arterial pressure waveform data along with a hybrid Adam-L-BFGS optimizer yielded the best results. It should be stated that a limitation of the proposed approach is that it is assumed that the 0-D model is complex enough to capture the dynamics of an actual human cardiovascular system, not only for synthetic data generation but also for inference purposes. Therefore, future work will entail using retrospective clinical data to validate the proposed inference modelling approach.

Author Contributions: Conceptualization: R. L, P.H and J. L; methodology: R. L; software: R. L; original draft preparation: R. L, J.vd.M, P.H and J. L; writing-review and editing: R. L, J.vd.M, P.H and J.L; formal analysis: R.L. All authors have read and agreed to the published version of the manuscript.

Funding: This research received no external funding.

Conflicts of Interest: The authors declare no conflict of interest.

References

[1] A. K. Keates, A. O. Mocumbi, M. Ntsekhe, K. Sliwa, and S. Stewart, "Cardiovascular disease in Africa: Epidemiological profile and challenges," *Nat. Rev. Cardiol.*, vol. 14, no. 5, pp. 273–293, 2017, doi: 10.1038/nrcardio.2017.19.

[2] M. F. Yuyun, K. Sliwa, A. P. Kengne, A. O. Mocumbi, and G. Bukhman, "Cardiovascular diseases in sub-saharan Africa compared to high-income countries: An epidemiological perspective," *Glob. Heart*, vol. 15, no. 1, pp. 1–18, 2020, doi: 10.5334/GH.403.

[3] M. T. Maeder *et al.*, "Pulmonary Hypertension in Aortic and Mitral Valve Disease," *Front. Cardiovasc. Med.*, vol. 5, no. May, pp. 1–15, 2018, doi: 10.3389/fcvm.2018.00040.

[4] S. Rosenkranz and I. R. Preston, "Right heart catheterisation: Best practice and pitfalls in pulmonary hypertension," *Eur. Respir. Rev.*, vol. 24, no. 138, pp. 642–652, 2015, doi: 10.1183/16000617.0062-2015.

[5] S. Parasuraman *et al.*, "Assessment of pulmonary artery pressure by echocardiography-A comprehensive review," *IJC Hear. Vasc.*, vol. 12, pp. 45–51, 2016, doi: 10.1016/j.ijcha.2016.05.011.

[6] M. R. Fisher *et al.*, "Accuracy of doppler echocardiography in the hemodynamic assessment of pulmonary hypertension," *Am. J. Respir. Crit. Care Med.*, vol. 179, no. 7, pp. 615–621, 2009, doi: 10.1164/rccm.200811-1691OC.

[7] C. Rackauckas *et al.*, "Universal Differential Equations for Scientific Machine Learning," pp. 1–55, 2020, [Online]. Available: http://arxiv.org/abs/2001.04385.

[8] N. L. Bjørdalsbakke, J. T. Sturdy, D. R. Hose, and L. R. Hellevik, "Parameter estimation for closed-loop lumped parameter models of the systemic circulation using synthetic data," *Math. Biosci.*, vol. 343, no. October 2021, p. 108731, 2022, doi: 10.1016/j.mbs.2021.108731.

[9] Z. Keshavarz-Motamed, "A diagnostic, monitoring, and predictive tool for patients with complex valvular, vascular and ventricular diseases," *Sci. Rep.*, vol. 10, no. 1, pp. 1–19, 2020, doi: 10.1038/s41598-020-63728-8.

[10] F. Huang and S. Ying, "On-line parameter identification of the lumped arterial system model: A simulation study," *PLoS One*, vol. 15, no. 7 July, pp. 1–17, 2020, doi: 10.1371/journal.pone.0236012.

[11] A. L. Colunga *et al.*, "Deep phenotyping of cardiac function in heart transplant patients using cardiovascular system models," *J. Physiol.*, vol. 598, no. 15, pp. 3203–3222, 2020, doi: 10.1113/JP279393.

[12] Mathworks, "fmincon," *fmincon: User guide*, 2022. https://www.mathworks.com/help/optim/ug/fmincon.html.

[13] SciPy Organisation, "SciPy 1.8.0: User guide," *scipy.optimize.least_squares*, 2021. https://docs.scipy.org/doc/scipy/reference/generated/scipy.optimize.least_squares.html.

[14] R. Laubscher, J. Van Der Merwe, J. Liebenberg, and P. Herbst, "Non-invasive estimation of left ventricle elastance using a multi-compartment lumped parameter model and gradient-based optimization with forward-mode automatic differentiation," 2022, [Online]. Available: http://arxiv.org/abs/2205.12330.

[15] A. L. Marsden, "Optimization in cardiovascular modeling," *Annu. Rev. Fluid Mech.*, vol. 46, no. September, pp. 519–546, 2014, doi: 10.1146/annurev-fluid-010313-141341.

[16] C. Rackauckas and Q. Nie, "DifferentialEquations.jl," *J. Open Res. Softw.*, vol. 5, no. 1, p. 15, 2017, [Online]. Available: https://diffeq.sciml.ai/stable/.

[17] J. Revels, M. Lubin, and T. Papamarkou, "Forward-Mode Automatic Differentiation in Julia," *arXiv:1607.07892*, 2016.

[18] P. Morgensen and A. Riseth, "Optim: A mathematical optimization package for Julia," *J. Open Source Softw.*, vol. 3, no. 24, p. 615, 2018.

[19] M. Innes, "Flux: Elegant Machine Learning with Julia," *J. Open Source Softw.*, 2018.
[20] T. Korakianitis and Y. Shi, "Numerical simulation of cardiovascular dynamics with healthy and diseased heart valves," *J. Biomech.*, vol. 39, no. 11, pp. 1964–1982, 2006, doi: 10.1016/j.jbiomech.2005.06.016.
[21] H. Suga, K. Sagawa, and A. A. Shoukas, "Load independence of the instantaneous pressure-volume ratio of the canine left ventricle and effects of epinephrine and heart rate on the ratio.," *Circ. Res.*, vol. 32, no. 3, pp. 314–322, 1973, doi: 10.1161/01.RES.32.3.314.
[22] T. Korakianitis and Y. Shi, "A concentrated parameter model for the human cardiovascular system including heart valve dynamics and atrioventricular interaction," *Med. Eng. Phys.*, vol. 28, no. 7, pp. 613–628, 2006, doi: 10.1016/j.medengphy.2005.10.004.
[23] S. Bozkurt, "Mathematical modeling of cardiac function to evaluate clinical cases in adults and children," *PLoS One*, vol. 14, no. 10, pp. 1–20, 2019, doi: 10.1371/journal.pone.0224663.
[24] R. Laubscher, J. van der Merwe, J. Liebenberg, and P. Herbst, "Dynamic simulation of aortic valve stenosis using a lumped parameter cardiovascular system model with flow regime dependent valve pressure loss characteristics," *Med. Eng. Phys.*, vol. 106, no. April, p. 103838, 2022, doi: 10.1016/j.medengphy.2022.103838.
[25] X. Zhang, D. Wu, F. Miao, H. Liu, and Y. Li, "Personalized Hemodynamic Modeling of the Human Cardiovascular System: A Reduced-Order Computing Model," *IEEE Trans. Biomed. Eng.*, vol. 67, no. 10, pp. 2754–2764, 2020, doi: 10.1109/TBME.2020.2970244.
[26] M. J. Kochenderfer and T. Wheeler, *Algorithms for Optimization*, 1st ed. Cambridge: MIT Press, 2019.
[27] W. Hager and H. Zhang, "CG_DESCENT, a conjugate gradient method with guaranteed descent," *ACM Trans. Math. Softw.*, vol. 32, pp. 113–137, 2006.
[28] J. Nocedal, "Updating Quasi-Newton Matrices with Limited Storage," *Math. Comput.*, vol. 35, no. 151, pp. 773–782, 1980.